IGS2023 $_{P}oster_{K}yleDuncan$

Kyle Duncan[1]

[1]Affiliation not available

June 16, 2023

The Seasonal Evolution of Sea Ice Deformation in the Arctic and Southern Oceans

Kyle Duncan[1], Sinéad L. Farrell[2,1], Eric Leuliette[3], and John Kuhn[3]

[1] Cooperative Institute for Satellite Earth System Studies, Earth System Science Interdisciplinary Center, University of Maryland, College Park, MD, USA, [2] Department of Geographical Sciences, University of Maryland, College Park, MD, USA
[3] NOAA Laboratory for Satellite Altimetry, NCWCP, College Park, MD, USA

kduncan@umd.edu

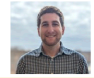

Introduction

ICESat-2's high-resolution photon counting lidar, with along-track sampling every 0.7 m, is providing unprecedented measurements of sea ice topography from a spaceborne altimeter, allowing for the detection of individual pressure ridges less than 10 m wide (Duncan & Farrell, 2022). Sea ice deformation features, such as pressure ridges, impact sea ice-atmosphere and sea ice-ocean momentum fluxes through ridge sails and keels, respectively, while also forming a major impediment to marine vessels. In this study we apply the University of Maryland-Ridge Detection Algorithm (UMD-RDA), a surface retracker, to detect pressure ridges and derive sea ice parameters such as surface roughness, ridge sail height, ridge width, sail width, ridging intensity, and ridge sail spacing, monthly, for both the Arctic and Southern Oceans.

University of Maryland – Ridge Detection Algorithm (UMD-RDA)

The UMD-RDA is a surface retracker applied to the ICESat-2 ATL03 Global Geolocated Photon Heights (Neumann et al., 2021) to extract sea ice surface height, as follows:

1. Running 5-shot (~2.8 m) photon aggregate is applied per shot, retaining nominal along-track sampling at 0.7 m
2. Photon height distribution (h) for each 5-shot aggregate is constructed and the modal height (h_m) is computed
3. Photon heights (h) are trimmed, retaining only photons that satisfy: $(h_m + 10\text{ m}) \geq h \geq (h_m - 2\text{ m})$ so as to capture ridge sails and leads, respectively
4. The height distribution is further trimmed, discarding data below the 15th and 85th percentiles so as to eliminate remaining background (noise) photons
5. The surface height is defined as the 99th percentile height of the remaining, fully trimmed height distribution.

Further info about UMD-RDA is in Duncan & Farrell (2022) https://doi.org/10.1029/2022GL100272

Although the UMD-RDA shows strong correlations with coincident airborne lidar data, the derivation of photon height from 5-shot aggregation results in an underestimate of total sail height by ~10 cm (Ricker et al., 2023).

Pressure Ridge Geometry

The UMD-RDA detects ridges by implementing the Rayleigh criterion. A ridge sail is simply the local maxima above the 60 cm cutoff height (to exclude snow deformation features) which is at least twice as high as the neighboring minima on either side and the minima descend at least halfway toward the local level ice surface. Ridges can therefore comprise multiple sails (Figure 1).

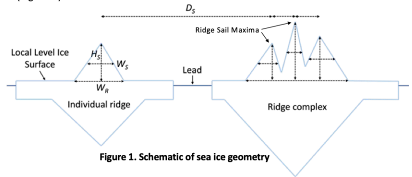

Figure 1. Schematic of sea ice geometry

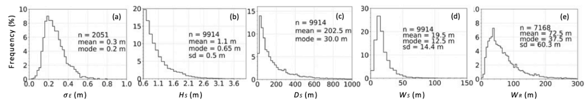

Figure 2. Surface deformation statistics derived by the UMD-RDA from ICESat-2 ATL03 data acquired on April 22, 2019, RGT 371, gt2l strong beam data. (a) Surface roughness (σ_E), (b) Sail height (H_S), (c) Sail spacing (D_S), (d) Sail width (W_S), and (e) Ridge width (W_R).

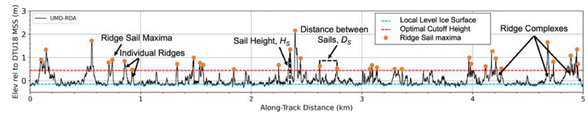

Sea Ice Parameters Detected with ICEsat-2

Sail Height (H_S)
Height above local level ice surface at ridge sail maxima

Ridge Width (W_R)
Distance between the points of intersection of the local level ice surface and the neighboring minima on either side of the ridge sail maxima

Sail Width (W_S)
Distance between points of intersection of a line, located at half the sail height, with the slope on the left and right of the sail maxima

Distance between Sails (D_S)
Peak-to-peak distance between consecutive sail maxima

Maximum Sail Height ($H_{S\,max}$)
Maximum sail height value per km

Ridging Intensity (I_R)
Mean sail height × sail frequency (per km)

Surface Roughness (σ_E)
Standard deviation of elevations within 1 km along-track segments

Figure 3. 5 km segment illustrating UMD-RDA surface topography and ridge metrics used in this study.

Arctic Ocean

Monthly Pan-Arctic Sea Ice Surface Roughness: Winter 2018/19 and 2020/21

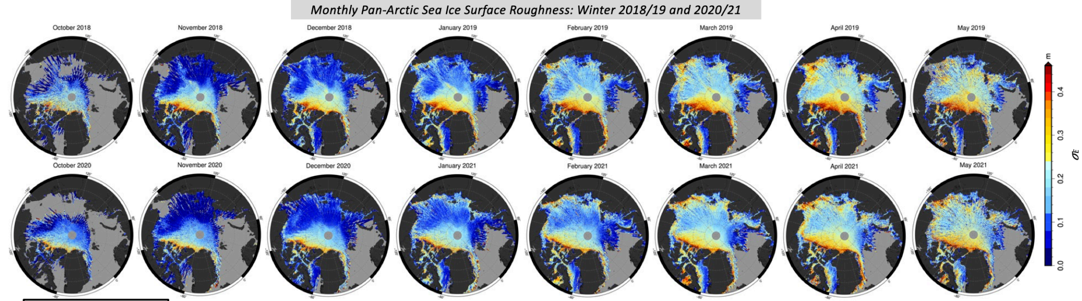

1 km data gridded at 1/12th degree

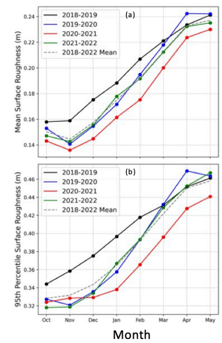

Figure 4. (a) Monthly mean surface roughness for the 2018/19 (black dots), 2019/20 (blue dots), 2020/21 (red dots), and 2021/22 (green dots) winter (Oct-May) seasons. The monthly mean for the entire 2018-2022 period (gray dashed line) is also shown. (b) Same as in (a) but for the 95th percentile of surface roughness.

Summary Results

- **Over the study period, surface roughness, maximum sail height and ridging intensity peaked in Apr. 2020, May 2019, and May 2022, but dropped to their lowest values in Aug. 2020, Oct. 2021, and Sep. 2020. Sail spacing reached a minimum in May 2020 and peaked in September 2020.**
- **Average surface roughness increases by ~8-10 cm during the 8 months of winter (Oct-May) and decreases by the same amount in just 4 months during summer (June-Sep).**
- **Pan-Arctic surface roughness was above average in winter 2018/19 but lower than average in winter 2020/21. The winters of 2019/20 and 2021/22 showed average conditions.**
- **During winter, maximum sail height increased ~25% and ridging intensity increased ~60-110%. Sail spacing decreased by ~50% during winter.**

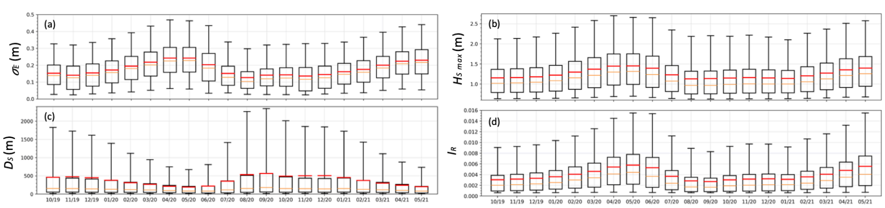

Figure 5. Box and whisker plots showing the monthly evolution of Arctic sea ice surface roughness for the period October 2019 to May 2021 (an entire winter-summer-winter cycle). (a) Surface roughness (σ_E), (b) Maximum sail height ($H_{S\,max}$), (c) Sail Spacing (D_S), and (d) Ridging intensity (I_R). Red line (orange line) indicates the mean (median) value.

Southern Ocean

Monthly Pan-Antarctic Sea Ice Surface Roughness: Winter 2019

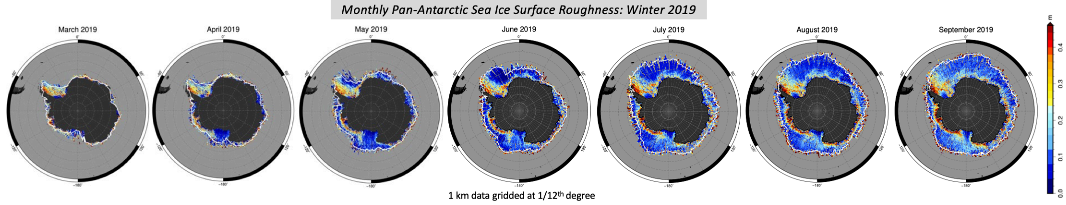

1 km data gridded at 1/12th degree

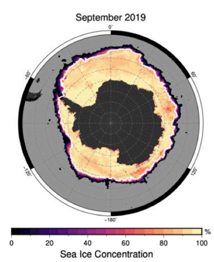

Figure 6. AMSR2 Antarctic sea ice concentration for September 2019. Solid white line denotes the 80% sea ice concentration contour.

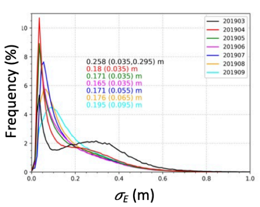

Figure 7. Probability distributions of monthly Antarctic sea ice surface roughness for the winter 2019 (March-September). Statistics show mean (modal) surface roughness.

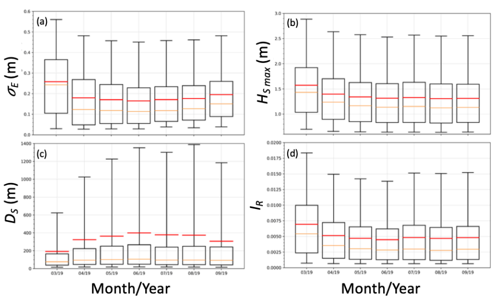

Figure 8. Box and whisker plots showing the monthly evolution of Antarctic sea ice surface roughness in winter 2019. (a) Surface roughness (σ_E), (b) Maximum sail height ($H_{S\,max}$), (c) Sail spacing (D_S), and (d) Ridging intensity (I_R). Red (orange) line indicates the mean (median) value.

AMSR2 daily sea ice concentration grids (Spreen et al., 2008) were averaged per month and used to derive the 80% contour line (white line, Figure 6 and in monthly maps). All data within this 80% contour line were used for further analysis while data outside this line was considered to be in the marginal ice zone (MIZ) and not used.

Summary Results

- **Seasonal evolution of surface roughness in the Southern Ocean in winter is in direct contrast to that of the Arctic, due to ice dynamics.**
- **Once ice extent nears its maximum and younger ice starts to slowly increase in roughness, surface deformation remains quite stable throughout the winter season.**
- **Antarctic surface roughness is dominated by perennial ice in March, with a quick decline in roughness as new, level ice forms in the months of April, May, and June.**

References

Duncan, K., & Farrell, S. L. (2022). Determining variability in Arctic sea ice pressure ridge topography with ICESat-2. Geophysical Research Letters, 49, e2022GL100272. https://doi.org/10.1029/2022GL100272

Ricker, R., Fons, S., Jutila, A., Hutter, N., Duncan, K., Farrell, S. L., Kurtz, N. T., and Fredensborg Hansen, R. M.: Linking scales of sea ice surface topography: evaluation of ICESat-2 measurements with coincident helicopter laser scanning during MOSAiC, The Cryosphere, 17, 1411–1429, https://doi.org/10.5194/tc-17-1411-2023, 2023.

Spreen, G., L. Kaleschke, and G. Heygster (2008), Sea ice remote sensing using AMSR-E 89 GHz channels, *J. Geophys. Res.*, vol. 113, C02S03, doi:10.1029/2005JC003384

This work is supported under NASA Cryosphere Program Grant 80NSSC20K0966 (ICESat-2 Science Team)